Research Article

Ying Li, Zhengkang Xu, Aili Jia, Xulin Yang*, Wei Feng, Pan Wang, Kui Li, Wenwu Lei, Hanyu He, Yingrui Tian, and Zuowan Zhou*

Controllable modification of helical carbon nanotubes for high-performance microwave absorption

https://doi.org/10.1515/ntrev-2021-0045
received May 12, 2021; accepted June 17, 2021

Abstract: Helical carbon nanotubes (HCNTs) are a kind of potential microwave absorption (MA) material due to their chiral and dielectric properties. However, the inert surface property makes HCNTs with poor polarization loss ability and impedance matching characteristic, which impedes its ability in attenuating microwaves. Herein, the HCNTs were modified with defects and functional groups on the surface to optimize their electromagnetic response characteristics and achieve an enhanced MA performance. The experimental results show that the modified HCNTs (F-HCNTs) exhibit a significant enhancement in MA performance when compared with HCNTs. The minimum reflection (RL_{min}) loss of F-HCNTs reaches −45.4 dB at 17.5 GHz at a thickness of 2.4 mm and the bandwidth of RL < −10 dB is 3.6 GHz (from 14.4 to 18.0 GHz). Further analysis demonstrates that proper modification of HCNTs leads to enhanced dielectric loss ability and optimized impedance matching characteristics, both of which are beneficial to the MA performance of HCNTs.

*** Corresponding author: Xulin Yang,** School of Mechanical Engineering, Chengdu University, 2025 Chengluo Avenue, Chengdu, 610106, China, e-mail: yangxulin@cdu.edu.cn
*** Corresponding author: Zuowan Zhou,** Institute of Frontier Science and Technology, Southwest Jiaotong University, Chengdu, 610031, China, e-mail: zwzhou@swjtu.edu.cn
Ying Li: School of Mechanical Engineering, Chengdu University, 2025 Chengluo Avenue, Chengdu, 610106, China; Key Laboratory of Advanced Technologies of Materials (Ministry of Education), School of Materials Science and Engineering, Southwest Jiaotong University, Chengdu, 610031, China
Zhengkang Xu, Aili Jia, Hanyu He, Yingrui Tian: Key Laboratory of Advanced Technologies of Materials (Ministry of Education), School of Materials Science and Engineering, Southwest Jiaotong University, Chengdu, 610031, China
Wei Feng, Pan Wang, Kui Li, Wenwu Lei: School of Mechanical Engineering, Chengdu University, 2025 Chengluo Avenue, Chengdu, 610106, China

Keywords: helical carbon nanotubes, structural adjustment, microwave absorption

1 Introduction

Chiral structures have been proved to be capable of attenuating microwaves, and many investigations have demonstrated that helical carbon nanotubes (HCNTs) exhibit good microwave absorption (MA) performance because of their chiral structure and dielectric properties [1–4]. Except for the resistance loss and polarization loss brought by the carbon component and polarization centers including defects edges and interfaces, the helical nanostructures can induce cross-polarization under continuous microwave irradiation that leads to resonance losses, which also contributes to attenuate the electromagnetic waves [5,6]. In addition, the HCNTs had the advantages of low density and small size, which makes it feasible to be applied in electromagnetic protection coatings. However, the inert surface property makes HCNTs with poor polarization loss ability and impedance matching characteristics [7,8], which impedes its MA performance. Based on the electromagnetic interference shielding and the relevant theories, the main mechanisms for attenuating microwaves are dielectric loss and magnetic loss, wherein the polarization loss plays a key role. The polarization centers include the dipoles, heterogeneous interfaces, and polarizable structures. At GHz frequency band, polarization centers including electric dipoles and interfaces absorb greatly microwaves because these cause the electric polarization centers to execute damped oscillations, and magnetic dipoles precess with damping under the torques produced by the microwave's magnetic field [9,10]. For HCNTs, the hexagonal rings are the main structure that offer resistance loss, the defects including pentagonal rings and heptagonal rings, and the edges that offer polarization loss are minority [11,12].

The mainstream approach to enhance the MA polarization loss and optimize the impedance matching characteristics is to form hybrid materials that incorporate magnetic or dielectric materials, such as ferrites, nickels, and polymers [13–15]. For example, Li *et al.* successfully fabricated porous nickel ferrite hollow nanospheres/helical carbon nanowires composites, where the minimal reflection loss (RL_{min}) and bandwidth (RL < −10 dB) were −33.94 dB at a thickness of 2.1 mm and 3.22 GHz (from 9.18 to 12.4 GHz), respectively [13]. Tian *et al.* introduced polyaniline to modify HCNTs and prepared a dual-chirality hierarchical structure. The experimental results show that the hierarchical hybrids exhibit significantly enhanced MA performance when compared with those of either pure polyaniline or HCNTs [16]. The polarization centers relax in the alternating electromagnetic field to transform the electromagnetic energy into other forms; thus, the newly formed hybrid structure and heterogeneous interfaces offer more sites to attenuate microwaves. In addition, by incorporating with other materials, the spatial structure can be designed to optimize the impedance characteristics and further enhance the MA performance [17,18]. To fabricate the HCNTs into composites or hybrids, a process of activating the HCNTs' surface to increase the surface activity is necessary [19]. During the process, some vacancies or functional groups are created on the HCNTs, and their dielectric properties are simultaneously changed. It can be predicted that the MA performance of HCNTs would change simultaneously, and this is a feasible way to tune and enhance the MA performance. However, the study about the effect of these processes on the MA performance and the potential microwave loss mechanism remains vacant. Here in this paper, the evaluation of the effect of the surface modification process on HCNTs' structure and properties was performed. The authors strongly believe that this study not only reveals the relationship between the surface structure and MA performance but also offers guidance for the researchers who work on HCNTs and the relative materials.

2 Experiments

2.1 Materials and methods

HCNTs were synthesized through the chemical vapor deposition method by acetylene decomposition over the as-obtained precursor that was prepared by the novel precipitation/sol-gel/reduction technique [20]. The obtained products were annealed and washed to remove the amorphous carbon and excessive precursors before using and noted as O-HCNTs. The F-HCNTs were prepared by immersing O-HCNTs in a bottle filled with an acid mixture (HNO_3/H_2SO_4 = 1/3 in volume) for a set time (0.5, 1.0, and 3.0 h). During this process, the bottle was put in ice bath (sonication with a power of 100 W). The F-HCNTs modified at different times were noted as F-HCNTs-X h.

2.2 Characterization and testing

X-ray diffraction patterns were recorded with an X-ray diffractometer (XRD, Philips X-30) with Cu Kα radiation (λ = 1.54056 Å). Scanning electron microscope (SEM, JEOL JSM-7800F) and transmission electron microscope (TEM, JEOL JEM-2100) were used to characterize the morphologies. Raman spectra were conducted on Renishaw InVia Reflex with an excitation wavelength of 532 nm. Fourier transform infrared spectroscopy (FTIR, Bruker Tensor II) was conducted with a spectral resolution of 2/cm. The electromagnetic parameters of the frequency range of 2–18 GHz were collected by the vector network analyzer (VNA, Agilent 15071C) by the coaxial-line method. The testing samples were prepared by blending the aerogel microspheres with a paraffin matrix in a weight ratio of 1:9 toroidal-shaped samples ϕ_{out} = 7.00 mm and ϕ_{in} = 3.04 mm.

3 Results and discussion

First, the morphological analysis was conducted to evaluate the effect of modification time. The HCNTs were synthesized using Fe-bearing compounds [20], and the morphology exhibits typical features: chirality and helicity. As shown in Figure 1a and inset, the single carbon nanotubes show a kink-like structure with a tube diameter of about 200 nm. It has been proved that the diameter is determined by the grain size of the catalysts [21,22]; thus, the uneven tube diameter should be ascribed to the grain size difference of the catalysts. Two coiled nanotubes growing from Fe catalyst particle can be observed from the inset image, demonstrating a typical symmetrical growth mode that causes a mirror image of the two nanotubes. After 0.5 h of mixed acid treating, the helical structure remains relatively intact (Figure 1b), while exhibits remarkable change after more than 1 h of treating. As shown in Figure 1c, the morphologies of F-HCNTs are destroyed, and almost all the symmetrical nanotubes were broken and hollow nozzles of HCNTs can be observed clearly. When extending the treating time to 3 h, the helical structure was

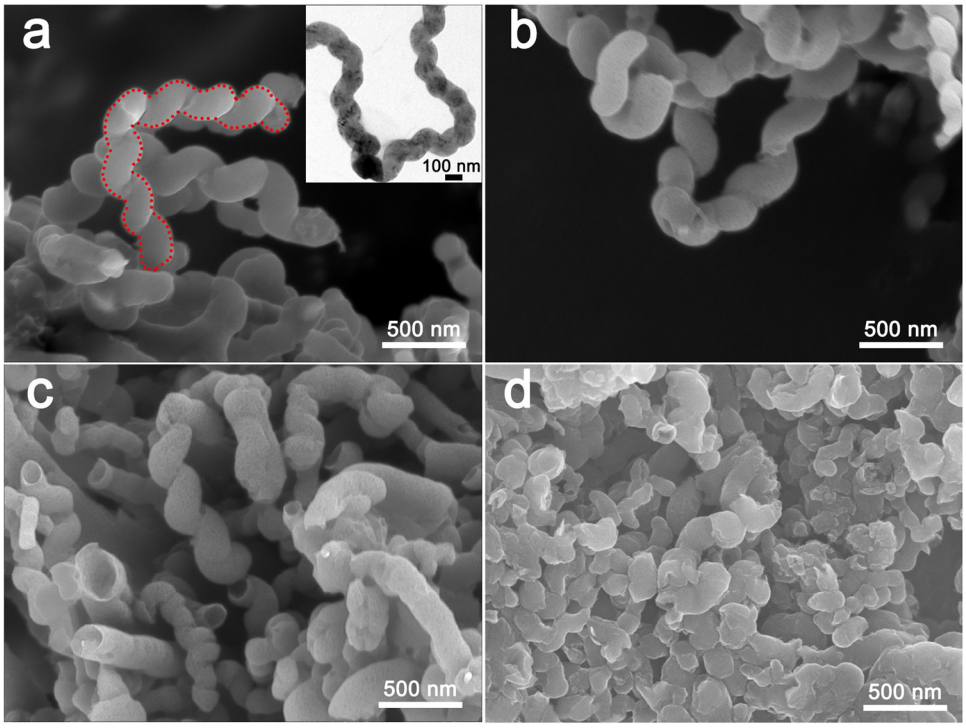

Figure 1: Morphological analysis of HCNTs. The SEM images of (a) O-HCNTs and (b–d) F-HCNTs treated for 0.5, 1, and 3 h.

destroyed. Excessive treating causes severe morphological destroy of F-HCNTs, and the structure is simultaneously changed.

Then, the Raman and FTIR spectra were performed to further analyze the structural information. It can be observed from the Raman spectra that the annealing treatment is effective to remove the amorphous carbon due to the I_D/I_G value of HCNTs drops from 1.79 to 1.30 after annealing (Figure 2a) [23,24]. It further confirmed the destructive effect of the mixed acid treatment on HCNTs for the I_D/I_G value gradually increases from 1.30 to 1.43. In addition, the mixed acid treating is also capable of oxidizing the carbon structure. The FTIR spectra show no significant change of HCNTs after annealing, while a new peak belonging to carboxyl groups appears around the 1,722/cm when treated by mixed acid for 0.5 h, implying the carboxyl groups has been grafted on the surface of F-HCNTs (Figure 2b) [25]. Except for the helical structures, the precursors inside HCNTs' tubes also offer electromagnetic loss mechanisms in MA performance. Thus, the XRD was applied to detect the existence of Fe. As shown in Figure 2c, there exhibits an obvious pattern of Fe after 3 h of treating, indicating the magnetic component is reserved [26].

Taking the magnetic component of HCNTs into account, it can be deduced that both dielectric loss and magnetic

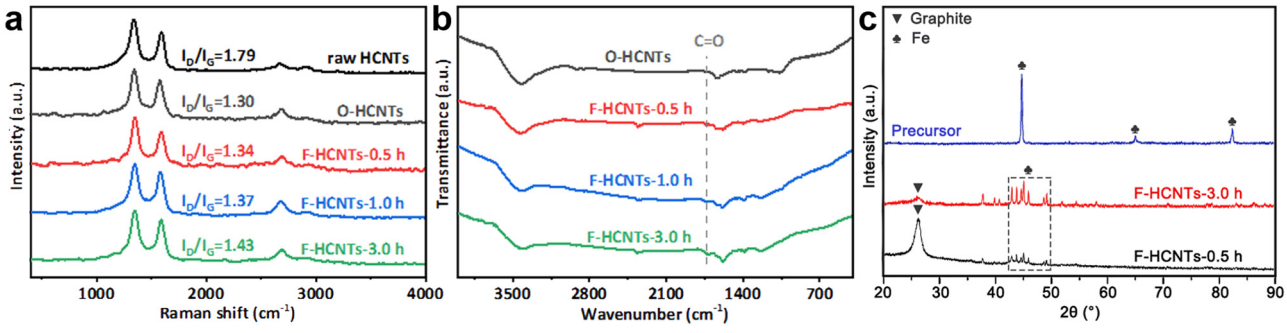

Figure 2: Structural analysis of HCNTs: (a) the Raman spectra, (b) the FT-IR spectra, and (c) the XRD patterns of O-HCNTs, F-HCNTs treated for 0.5, 1, and 3 h.

loss play key roles in electromagnetic absorption [27]. Along with the chemical treatment, the structural evolution leads to changes in dielectric and magnetic properties that relate to the MA performance. Therefore, the complex permittivity including real part (ε') and imaginary part (ε'') and the complex permeability including real part (μ') and imaginary part (μ'') of HCNTs in the frequency range of 2.0–18.0 GHz was collected by the vector network analyzer through the coaxial-line method. ε' represents absorbers' capacity of storing electromagnetic energy, and an increase indicates that the material is easier to be polarized under an external magnetic/electrical field and to store the energy [28,29]. As shown in Figure 3a, the ε' of F-HCHTs is lower than O-HCNTs, which indicates a weakened energy storage ability. The ε' shows a downward trend with the increase of frequency, which can be comprehended by the increased lagging of polarization with respect to electric-field change at higher frequency [30]. The ε'' stands for the dissipation ability of absorbers [31]. As depicted in Figure 3b, ε'' of F-HCNTs shows a small decrease in 2.0–14.4 GHz and an increase in 14.4–18.0 GHz when compared with O-HCNTs. For ε'' in the lower frequency band is mainly related to the resistance loss and in higher frequency band relates to the dielectric loss, which indicates that the modification process weakens the resistance loss ability of F-HCNTs due to the destroyed carbon structure [32,33]. However, the newly formed surface groups and defects on F-HCNTs are beneficial to enhance the dielectric loss ability that attenuates the electromagnetic waves at a higher frequency band. Benefits from the surface groups and defects that offers polarization centers, the F-HCNTs show an improvement in the capacity of converting electromagnetic wave energy to other forms in the range of 14–18 GHz as described by dielectric dissipation factors ($\tan\delta_\varepsilon = \varepsilon''/\varepsilon'$) (Figure 3c) [34]. Except for the dielectric loss part, the HCNTs also exhibit the ability in magnetic loss due to the helical structure and the existence of magnetical precursor. The complex permeability *versus* frequency curves exhibits several fluctuations in the 13–18 GHz as the complex permittivity does, which implies multiple magnetic loss behaviors and the capacity in storing and converting electromagnetic energy of the HCNTs (Figure 3d–f). Although the helical structure of F-HCNTs was certainly destroyed, the uncovered precursor inside the nanotubes simultaneously forms enhanced hysteresis including the multiple resonance effect, nature, and exchange resonance that attributes to the magnetic loss. It can be seen that the fluctuations appear at the high-frequency band, indicating a stronger attenuation ability at the high-frequency band.

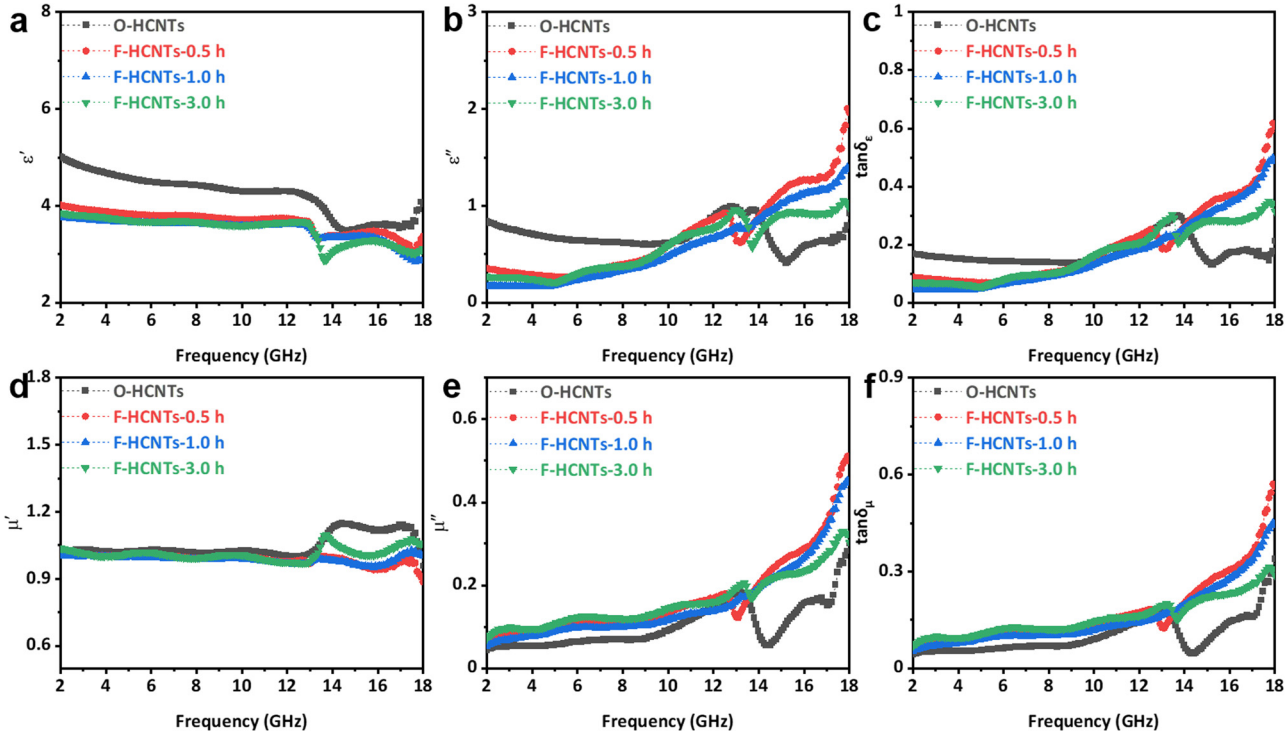

Figure 3: Measured frequency dependence of (a) ε', (b) ε'', (c) $\tan\delta_\varepsilon$, (d) μ', (e) μ'', and (f) $\tan\delta_\mu$ of O-HCNTs and F-HCNTs.

The MA performance is closely related to the electromagnetic parameters; thus, the MA performance was evaluated to further verify the above speculation. Based on parameters, the reflection loss (RL) was calculated by equations (1) and (2), where Z_{in} is the input characteristic impendence, Z_0 is the free space impendence, μ and ε are the measured complex permeability and complex permittivity, respectively, d is the thickness of the tested sample, c is the propagation velocity of microwave in free space, and f is the frequency of microwave [35].

$$\mathrm{RL} = 20\lg\left[\frac{(Z_{in} - Z_0)}{(Z_{in} + Z_0)}\right], \tag{1}$$

$$Z_{in} = Z_0\sqrt{\mu/\varepsilon}\,\tanh[\mathrm{j}(2\pi fd/c\sqrt{\mu\varepsilon})]. \tag{2}$$

As shown in Figure 4a, the pristine O-HCNTs barely meet the practical requirement of –10.0 dB [36], while undergoing the functionalization processing the F-HCNTs exhibits significantly enhanced MA capacity. When treated for 0.5 h, the minimal RL (RL_{min}) reaches –43.0 dB at 17.0 GHz with a thickness of 2.5 mm and a bandwidth of RL < –10 dB is 4.0 GHz (from 14.0 to 18.0 GHz) (Figure 4b). When further elongating the treating time for 1 h, the MA performance has a slight increase that the RL_{min} reaches –45.4 dB at 17.5 GHz with a thickness of 2.4 mm and a bandwidth of RL < –10 dB is 3.6 GHz (from 14.4 to 18.0 GHz) (Figure 4c). These results are consistent with the testing electromagnetic parameters, which will be further analyzed later. However, when increasing the treating time to 3.0 h, the RL significantly decreases. As illustrated in Figure 4d, the optimized RL_{min} reaches –20.2 dB at 17.7 GHz with a thickness of 2.5 mm and a bandwidth of RL < –10 dB is 3.4 GHz (from 14.6 to 18.0 GHz).

The MA performance is closely affected by the loss characteristics. To explain why the MA performance of HCNTs changes with the treating time, further analysis on the electromagnetic parameters is performed. First, the loss mechanism is studied based on the Debye theory, which is described as the following equations [37]:

$$\left(\varepsilon' - \frac{\varepsilon_s + \varepsilon_\infty}{2}\right)^2 + (\varepsilon'')^2 = \left(\frac{\varepsilon_s + \varepsilon_\infty}{2}\right)^2, \tag{3}$$

where ε_s is the static dielectric constant, ε_∞ refers to the dielectric constant at infinite frequency, and τ indicates

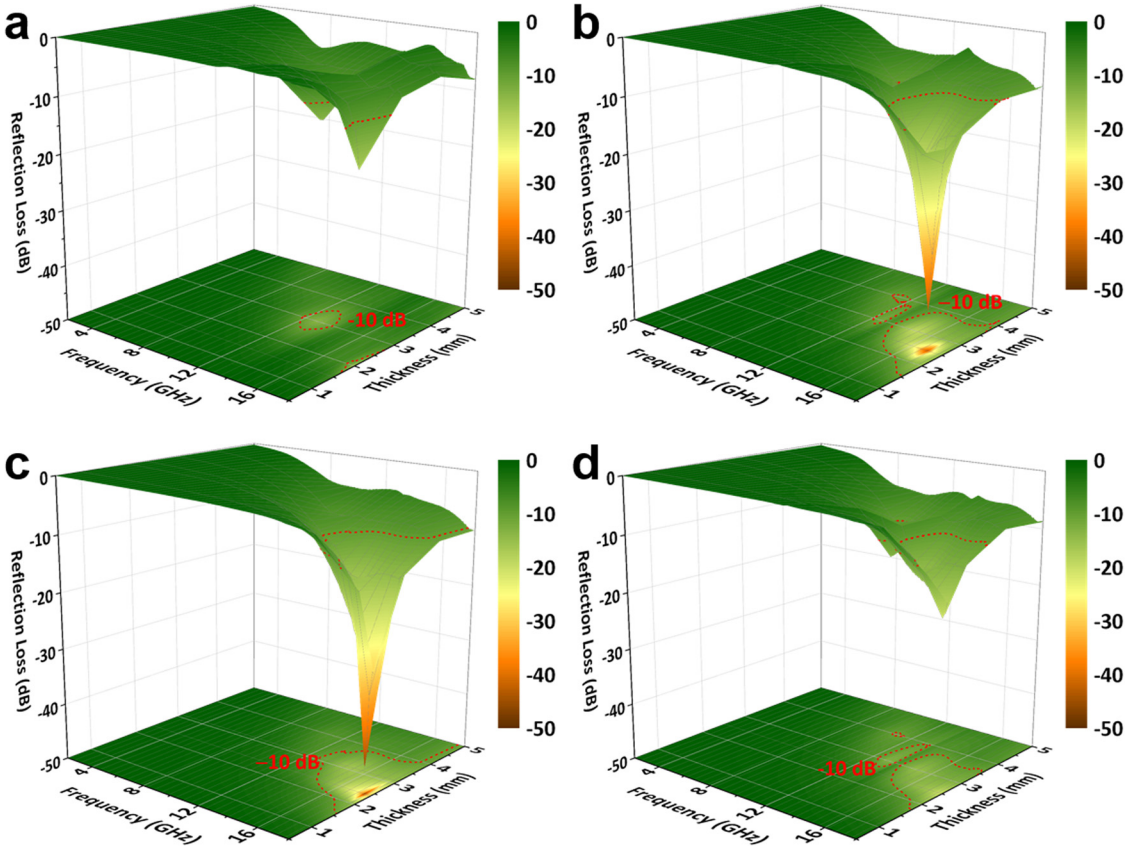

Figure 4: The calculated reflection loss of HCNTs. (a) A-HCNTs, (b–d) F-HCNTs-0.5 h, F-HCNTs-1.0 h, and F-HCNTs-3.0 h, respectively.

polarization relaxation time, respectively. The ε' and ε'' can be expressed by formulas (4) and (5) [38]

$$\varepsilon' = \varepsilon_\infty + \frac{\varepsilon_s - \varepsilon_\infty}{1 + (j2\pi)^2\tau^2}, \tag{4}$$

$$\varepsilon'' = \frac{2\pi f\tau(\varepsilon_s - \varepsilon_\infty)}{1 + (2f\pi)^2\tau^2}. \tag{5}$$

Figure 5a depicts the Cole–Cole semicircles. Every semicircle represents a relaxation process; thus, the multiple semicircles for all the F-HCNTs imply the presence of multi-dielectric relaxations [39,40]. Meanwhile, the number of semicircles increases as treating time increases, indicating there exists more newly formed loss mechanisms on F-HCNTs. In addition, the more multiple semicircles of F-HCNTs indicate more loss mechanisms over O-HCNTs. For carbon nanotubes, the main mechanism of dielectric loss includes resistance loss at lower frequency band, polarization relaxation loss, interfaces polarization loss, and dielectric structural loss and resonance loss at higher frequency band. From Figure 3c, it can be concluded that the loss mechanism transfer from dielectric loss to polarization loss as the increasing frequency of all the F-HCNTs. The special spatial conformation of the HCNTs and the surface modification process that brings more defects and polarization centers leads to enhanced dielectric loss mechanisms at high-frequency bands. While for O-HCNTs, the tan δ_ε at lower frequency band is higher than F-HCNTs, which means O-HCNTs possess stronger resistance loss ability. This explains the phenomenon of O-HCNTs that exist a longer tail at the curve end. An excellent MA performance should be obtained only when the material has both loss characterization and impedance matching at the same time [32,41,42]. To explain the superior MA performance of F-HCNTs-1.0 h to the others, first, the loss characterization (attenuation constant, α) is evaluated by equation (6) (Figure 5b) [43]. It can be found that α of F-HCNTs shows an enhanced trend over O-HCNTs at the higher frequency band (about 14–18 GHz) and a slightly weaken trend at the lower frequency band. This indicates that surface modification is beneficial to enhance the dielectric loss ability. Eddy currents exist in the material that permeates in the alternate electromagnetic field, and it would be detrimental to the material's attenuating ability. Thus, the eddy currents should be avoided [14,44]. The C_0 value is calculated based on equation (7) to evaluate the effect of eddy currents [45]. As shown in Figure 5c, F-HCNTs show almost a constant in the measured frequency, indicating a negligible eddy current effect. Second, the impedance matching degree (delta, Δ) is further evaluated by equation (8), in which the K and M can be calculated from the relative permittivity and relative permeability by equations (9) and (10), respectively [46]. According to the impedance matching theory, the impedance matching degree should be equal or close to that of free space at the interface between MA absorbers

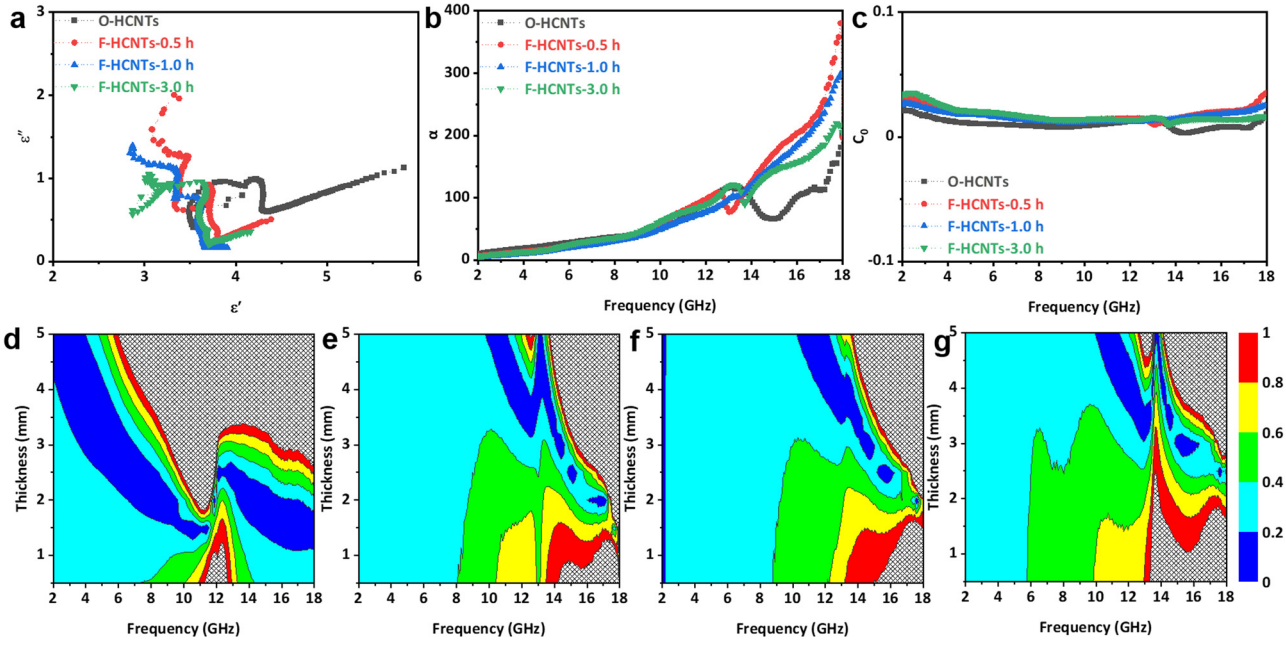

Figure 5: Analysis of the electromagnetic parameters: (a) Cole–Cole curves, (b) attenuation factors, (c) C_0, and (d–f) the impedance matching degree of O-HCNTs, F-HCNTs-0.5 h, F-HCNTs-1.0 h, and F-HCNTs-3.0 h, respectively.

and free space. Impedance mismatching would cause reflection or transmission of most electromagnetic waves, a Δ value smaller than 0.4 is considered acceptable for MA performance [47]. As presented in Figure 5d–g, the F-HCNTs possess larger area than O-HCNTs, indicating an enhanced impedance matching degree over the O-HCNTs. This further explains why the F-HCNTs exhibit better MA performance over O-HCNTs.

$$\alpha = \frac{\sqrt{2}\pi f}{c} \times \sqrt{(\mu''\varepsilon'' - \mu'\varepsilon') + \sqrt{(\mu''\varepsilon'' - \mu'\varepsilon')^2 + (\mu''\varepsilon'' + \mu'\varepsilon')^2}}, \quad (6)$$

$$C_0 = \frac{\mu''}{(\mu')^2 f}, \quad (7)$$

$$\Delta = |\sinh^2(Kfd) - M|, \quad (8)$$

$$K = 4\frac{\pi\sqrt{\mu'\varepsilon'}\sin\left(\frac{\varepsilon+\mu}{2}\right)}{c \cdot \cos\varepsilon \cdot \cos\mu}, \quad (9)$$

$$M = 4\frac{\mu'\varepsilon'\cos\varepsilon \cdot \cos\mu}{(\mu'\cos\varepsilon - \varepsilon'\cos\mu)^2 + \tan^2\left(\frac{\varepsilon-\mu}{2}\right) \cdot (\mu'\cos\varepsilon + \varepsilon'\cos\mu)^2}. \quad (10)$$

Based on the above analysis, the difference in MA performance among HCNTs can be explained. O-HCNTs have relatively higher resistance loss ability than the F-HCNTs, while their polarization loss ability is weak due to the fewer polarization centers. Besides, the impedance matching degree of O-HCNTs is poor, these factors make O-HCNTs exhibit relatively poor MA performance than F-HCNTs. For F-HCNTs-0.5 h whose surface is covered by functional groups and defects, the newly formed heterogeneous structure offers polarization centers to attenuate microwaves. In addition, the treating process changes the dielectric properties of HCNTs, reserves its resistance loss ability, and optimizes its impedance matching degree to enhance the MA performance. When elongating the treating time to 1 h, more functional groups and defects appear on the surface of HCNTs, resulting in enhanced polarization loss ability and optimized impedance matching degree. However, 3 h of treating seriously destroys the structure of HCNTs and the dielectric loss ability drops obviously, leading to poor MA performance. In conclusion, the excellent MA performance of F-HCNTs should be attributed to its optimized impedance matching and high attenuation constant, mainly due to the outstanding dielectric loss generated from the defects, surface groups, residue precursors, and resistance loss and interfacial polarization of HCNTs. A possible MA mechanism of HCNTs is presented in Figure 6.

4 Conclusion

In summary, this paper synthesized functional helical carbon nanotubes (F-HCNTs) and evaluated their ability and mechanism of attenuating microwaves. The F-HCNTs show an enhanced microwave absorption (MA) performance compared to HCNTs. The optimized minimal reflection loss (RL_{min}) of F-HCNTs reaches −45.4 dB at 17.5 GHz with a thickness of 2.4 mm and bandwidth of

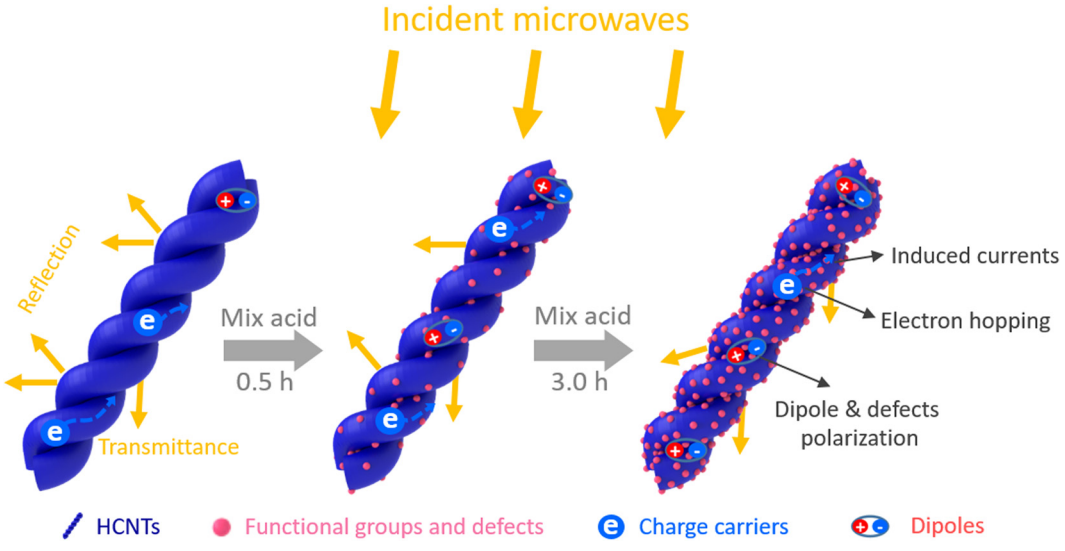

Figure 6: Schematic illustration of the potential MA mechanisms for HCNTs.

RL < −10 dB is 3.6 GHz (from 14.4 to 18.0 GHz). Structural characterization demonstrated that functional groups and defects were formed on HCNTs' surface when treated by an acid mixture. Enhanced MA performance can be ascribed to the newly formed polarization centers and optimized impedance matching characteristics. The cooperation of the relaxations from functional groups and defects synergistically enhances the dielectric loss ability. In addition, the MA performance could simply be controlled by tuning the treating time of the HCNTs. The authors believe that this article will provide a new pathway toward the controllable design of high-performance or multifunctional devices based on helical carbon nanostructures and their hybrids.

Funding information: This work was financially supported by the Opening Foundation of Sichuan Province Engineering Research Center for Powder Metallurgy (SCFMYJ2020-04), Applied Basic Research Programs of Sichuan province (2018JY0062), and Chengdu Technology Innovation Research and Development Project (2019-YFYF-00013-SN).

Author contributions: All authors have accepted responsibility for the entire content of this manuscript and approved its submission.

Conflict of interest: The authors state no conflict of interest.

References

[1] Li KY, Sun H, Zhang X, Zhang S, Dong HW, Zhu CL, et al. Micronanospheres assembled with helically coiled nitrogen-doped carbon nanotubes: fabrication and microwave absorption properties. Mater Design. 2020;186:108290.

[2] Qi X, Yang E, Cai H, Xie R, Bai Z, Jiang Y, et al. Water-assisted and controllable synthesis of core/shell/shell structured carbon-based nanohybrids, and their magnetic and microwave absorption properties. Sci Rep. 2017;7(1):9851.

[3] Barathi Dassan EG, Anjang Ab Rahman A, Abidin MSZ, Akil HM. Carbon nanotube–reinforced polymer composite for electromagnetic interference application: a review. Nanotechnol Rev. 2020;9(1):768–88.

[4] Lau KT, Lu M, Hui D. Coiled carbon nanotubes: synthesis and their potential applications in advanced composite structures. Compos Part B Eng. 2006;37(6):437–48.

[5] Wu F, Yang K, Li Q, Shah T, Ahmad M, Zhang Q, et al. Biomass-derived 3D magnetic porous carbon fibers with a helical/chiral structure toward superior microwave absorption. Carbon. 2021;173:918–31.

[6] Wu F, Liu Z, Xiu T, Zhu B, Khan I, Liu P, et al. Fabrication of ultralight helical porous carbon fibers with CNTs-confined Ni nanoparticles for enhanced microwave absorption. Compos Part B Eng. 2021;215:108814.

[7] Selim MM, El-Safty SA. Vibrational analysis of an irregular single-walled carbon nanotube incorporating initial stress effects. Nanotechnol Rev. 2020;9(1):1481–90.

[8] Dong M, Peng M, Wei W, Xu H, Liu C, Shen C. Improved microwave absorption performance of double helical C/Co@CNT nanocomposite with hierarchical structures. J Mater Chem C. 2021;9(6):2178–89.

[9] Ulloa RZ, Santiago MGH, Rueda VLV. The interaction of microwaves with materials of different properties. London: IntechOpen; 2019.

[10] Wang C, Murugadoss V, Kong J, He ZF, Mai XM, Shao Q, et al. Overview of carbon nanostructures and nanocomposites for electromagnetic wave shielding. Carbon. 2018;140:696–733.

[11] Xu HL, Yin XW, Fan XM, Tang ZM, Hou ZX, Li MH, et al. Constructing a tunable heterogeneous interface in bimetallic metal-organic frameworks derived porous carbon for excellent microwave absorption performance. Carbon. 2019;148:421–9.

[12] Zhang D, Hao Z, Qian Y, Huang Y, Bizeng, Yang Z, et al. Simulation and measurement of optimized microwave reflectivity for carbon nanotube absorber by controlling electromagnetic factors. Sci Rep. 2017;7(1):479.

[13] Li LD, Lu LF, Qi SH. Preparation, characterization and microwave absorption properties of porous nickel ferrite hollow nanospheres/helical carbon nanotubes/polypyrrole nanowires composites. J Mater Sci-Mater El. 2018;29(10):8513–22.

[14] Zhao B, Li Y, Zeng Q, Wang L, Ding J, Zhang R, et al. Galvanic replacement reaction involving core-shell magnetic chains and orientation-tunable microwave absorption properties. Small. 2020;16(40):e2003502.

[15] Zhao Y, Zhang H, Yang X, Huang H, Zhao G, Cong T, et al. In situ construction of hierarchical core–shell Fe3O4@C nanoparticles–helical carbon nanocoil hybrid composites for highly efficient electromagnetic wave absorption. Carbon. 2021;171:395–408.

[16] Tian X, Meng F, Meng F, Chen X, Guo Y, Wang Y, et al. Synergistic enhancement of microwave absorption using hybridized polyaniline@helical CNTs with dual chirality. ACS Appl Mater Interfaces. 2017;9(18):15711–8.

[17] Singh SK, Akhtar MJ, Kar KK. Hierarchical carbon nanotube-coated carbon fiber: ultra lightweight, thin, and highly efficient microwave absorber. ACS Appl Mater Interfaces. 2018;10(29):24816–28.

[18] Wang T, Shi M, Fang D, He J, Zhang M, Zhang S, et al. Novel spiro[fluorene-9,9′-xanthene]-based hole transport layers for red and green PHOLED devices with high efficiency and low efficiency roll-off. J Mater Chem C. 2021;9(9):3247–56.

[19] Yang X, Peng Y, Hou J, Liu Y, Jian X. A review for modified Li composite anode: principle, preparation and challenge. Nanotechnol Rev. 2020;9(1):1610–24.

[20] Meng FB, Wang Y, Wang Q, Xu XL, Jiang M, Zhou XS, et al. High-purity helical carbon nanotubes by trace-water-assisted chemical vapor deposition: large-scale synthesis and growth mechanism. Nano Res. 2018;11(6):3327–39.

[21] Tang N, Wen J, Zhang Y, Liu F, Lin K, Du Y. Helical carbon nanotubes: catalytic particle size-dependent growth and magnetic properties. Acs Nano. 2010;4(1):241–50.

[22] Pant M, Singh R, Negi P, Tiwari K, Singh Y. A comprehensive review on carbon nano-tube synthesis using chemical vapor deposition. Mater Today Proc. 2021. doi: 10.1016/j.matpr.2021.02.646.

[23] Fang B, Chang D, Xu Z, Gao C. A review on graphene fibers: expectations, advances, and prospects. Adv Mater. 2020;32(5):e1902664.
[24] Tian W, Zhang X, Guo Y, Mu C, Zhou P, Yin L, et al. Hybrid silica-carbon bilayers anchoring on FeSiAl surface with bifunctions of enhanced anti-corrosion and microwave absorption. Carbon. 2021;173:185–93.
[25] Yengejeh SI, Kazemi SA, Ochsner A. Carbon nanotubes as reinforcement in composites: a review of the analytical, numerical and experimental approaches. Comp Mater Sci. 2017;136:85–101.
[26] Almessiere MA, Slimani Y, Trukhanov AV, Sadaqat A, Korkmaz AD, Algarou NA, et al. Review on functional bi-component nanocomposites based on hard/soft ferrites: structural, magnetic, electrical and microwave absorption properties. Nano-Struct Nano-Objects. 2021;26:100728.
[27] Zhang Z, Cai Z, Wang Z, Peng Y, Xia L, Ma S, et al. A review on metal–organic framework-derived porous carbon-based novel microwave absorption materials. Nano-Micro Let. 2021;13:1.
[28] Li Y, Meng F, Mei Y, Wang H, Guo Y, Wang Y, et al. Electrospun generation of Ti3C2Tx MXene@graphene oxide hybrid aerogel microspheres for tunable high-performance microwave absorption. Chem Eng J. 2020;391:123512.
[29] Gu WH, Sheng JQ, Huang QQ, Wang GH, Chen JB, Ji GB. Environmentally friendly and multifunctional shaddock peel-based carbon aerogel for thermal-insulation and microwave absorption. Nano-Micro Let. 2021;13(1):1–14.
[30] Quan B, Liang X, Ji G, Ma J, Ouyang P, Gong H, et al. Strong electromagnetic wave response derived from the construction of dielectric/magnetic media heterostructure and multiple interfaces. ACS Appl Mater Interfaces. 2017;9(11):9964–74.
[31] Wu N, Hu Q, Wei R, Mai X, Naik N, Pan D, et al. Review on the electromagnetic interference shielding properties of carbon based materials and their novel composites: Recent progress, challenges and prospects. Carbon. 2021;176:88–105.
[32] Liu Y, Jiang L, Wang H, Wang H, Jiao W, Chen G, et al. A brief review for fluorinated carbon: synthesis, properties and applications. Nanotechnol Rev. 2019;8(1):573–86.
[33] Li XL, Yin XW, Han MK, Song CQ, Xu HL, Hou ZX, et al. Ti_3C_2 MXenes modified with in situ grown carbon nanotubes for enhanced electromagnetic wave absorption properties. J Mater Chem C. 2017;5(16):4068–74.
[34] Zhou J, Chen Y, Li H, Dugnani R, Du Q, UrRehman H, et al. Facile synthesis of three-dimensional lightweight nitrogen-doped graphene aerogel with excellent electromagnetic wave absorption properties. J Mater Sci. 2017;53(6):4067–77.
[35] Wang C, Wang B, Cao X, Zhao J, Chen L, Shan L, et al. 3D flower-like Co-based oxide composites with excellent wide-band electromagnetic microwave absorption. Compos Part B Eng. 2021;205(30):108529.
[36] Wei HJ, Yin XW, Li X, Li MH, Dang XL, Zhang LT, et al. Controllable synthesis of defective carbon nanotubes/Sc2Si2O7 ceramic with adjustable dielectric properties for broadband high-performance microwave absorption. Carbon. 2019;147:276–83.
[37] Xu HL, Yin XW, Li MH, Ye F, Han MK, Hou ZX, et al. Mesoporous carbon hollow microspheres with red blood cell like morphology for efficient microwave absorption at elevated temperature. Carbon. 2018;132:343–51.
[38] Wang H, Meng F, Huang F, Jing C, Li Y, Wei W, et al. Interface modulating CNTs@PANi hybrids by controlled unzipping of the walls of CNTs to achieve tunable high-performance microwave absorption. ACS Appl Mater Interfaces. 2019;11(12):12142–53.
[39] Jia Z, Zhang M, Liu B, Wang F, Wei G, Su Z. Graphene foams for electromagnetic interference shielding: a review. ACS Appl Nano Mater. 2020;3(7):6140–55.
[40] Green M, Chen XB. Recent progress of nanomaterials for microwave absorption. J Mater. 2019;5(4):503–41.
[41] Quan B, Liang XH, Ji GB, Cheng Y, Liu W, Ma JN, et al. Dielectric polarization in electromagnetic wave absorption: review and perspective. J Alloys Compd. 2017;728:1065–75.
[42] Xie J, Jiang H, Li J, Huang F, Zaman A, Chen X, et al. Improved impedance matching by multi-componential metal-hybridized rGO toward high performance of microwave absorption. Nanotechnol Rev. 2021;10(1):1–9.
[43] Li T, Zhi DD, Chen Y, Li B, Zhou ZW, Meng FB. Multiaxial electrospun generation of hollow graphene aerogel spheres for broadband high-performance microwave absorption. Nano Res. 2020;13(2):477–84.
[44] Lv H, Zhang H, Ji G, Xu ZJ. Interface strategy to achieve tunable high frequency attenuation. ACS Appl Mater Interfaces. 2016;8(10):6529–38.
[45] Du S, Chen H, Hong R. Preparation and electromagnetic properties characterization of reduced graphene oxide/strontium hexaferrite nanocomposites. Nanotechnol Rev. 2020;9(1):105–14.
[46] Zhi D, Li T, Li J, Ren H, Meng F. A review of three-dimensional graphene-based aerogels: synthesis, structure and application for microwave absorption. Compos Part B Eng. 2021;211:108642.
[47] Xu X, Shi S, Tang Y, Wang G, Zhou M, Zhao G, et al. Growth of NiAl-layered double hydroxide on graphene toward excellent anticorrosive microwave absorption application. Adv Sci (Weinh). 2021;8(5):2002658.